Optics and Laser Technology 112 (2019) 442–451

Contents lists available at ScienceDirect

Optics and Laser Technology

journal homepage: www.elsevier.com/locate/optlastec

Full length article

2 Tb/s all-optical gates based on two-photon absorption in quantum dot semiconductor optical amplifiers

Amer Kotb[a,b,*], Kyriakos E. Zoiros[c], Chunlei Guo[a,d,*]

[a] The Guo China-US Photonics Laboratory, Changchun Institute of Optics, Fine Mechanics, and Physics, Chinese Academy of Sciences, Changchun 130033, China
[b] Department of Physics, Faculty of Science, University of Fayoum, Fayoum 63514, Egypt
[c] Lightwave Communications Research Group, Department of Electrical and Computer Engineering, School of Engineering, Democritus University of Thrace, Xanthi 67100, Greece
[d] The Institute of Optics, University of Rochester, Rochester, NY 14627, USA

HIGHLIGHTS

- Nonlinear effect of TPA on all-optical gates are realized using QDSOA at 2 Tb/s.
- Impact of critical performance parameters on QF is numerically analyzed.
- All-optical operations are executed with the employed scheme with twice as high QF than without TPA.

ARTICLE INFO

Keywords:
All-optical logic gates
Two-photon absorption
Quantum dot semiconductor optical amplifier
Mach-Zehnder interferometer
Delayed interferometer

ABSTRACT

The performance of all-optical AND, OR, and NAND gates based on quantum dot semiconductor optical amplifiers (QDSOAs), which are either incorporated in properly configured Mach-Zehnder interferometer or combined with a delayed interferometer, is theoretically investigated at a data rate of 2 Tb/s when the nonlinear effect of two-photon absorption (TPA) is exploited in these active devices. The impact of the input signal and QDSOA key parameters on the quality factor (QF) is assessed. The obtained results indicate that these Boolean functions can be executed at 2 Tb/s with almost as twice as high QF than without TPA.

1. Introduction

In recent years, semiconductor optical amplifiers (SOAs) have been established as dominant optoelectronic devices owing to their strong nonlinearity, small size, and ease of integration with other photonic elements. In particular, SOAs have been widely used to realize all-optically (AO) Boolean functions at different data rates [1–25]. However, SOAs inherently have slow gain and phase recovery times, which limit their signal processing capability for AO gating purposes to single-channel data rates that hardly exceed ~100 Gb/s. These physical limitations can be overcome via two-photon absorption (TPA) nonlinear effect, which can induce significant and ultrafast gain and phase changes exploitable for AO purposes [26]. In fact, leveraging TPA in SOAs has allowed extending the speed of AO logic operations at 250 Gb/s, as numerically investigated and shown in [27–31].

On the other hand, placing quantum dots (QDs) in the SOA active region results in shorter carrier relaxation time and lower gain saturation as a direct by-product of the gap between the QDs energy levels and the extra-formed wetting layer (WL) [17]. The gain recovery time of QDSOA is faster (i.e. 300 fs–10 ps) than bulk and quantum-well SOA. This QDSOAs attractive feature has been exploited in the theoretical demonstration of ultrafast AO logic gates realization using QDSOAs [32–45]. In this paper, we have combined the physical advantages of both TPA and QD to theoretically realize AO AND, OR, and NAND gates at 2 Tb/s, in line with upgraded data rates in modern lightwave networks [46]. The employed model considers the wetting layer (WL) carriers refilling by TPA as well as the nonlinear effects that affect the QDSOAs gain and phase dynamics. To the best of our knowledge, the performance of the considered AO gates has not been addressed so far using QDSOA with induced TPA at 2 Tb/s. The core switching unit used for implementing the AND and NAND gates is the Mach-Zehnder Interferometer (MZI), which has two symmetrical QDSOAs in its two arms, while the OR gate is constructed by combining a QDSOA with a Delayed Interferometer (DI). The dependence of the

* Corresponding authors at: The Guo China-US Photonics Laboratory, Changchun Institute of Optics, Fine Mechanics, and Physics, Chinese Academy of Sciences, Changchun 130033, China.
E-mail addresses: amer@ciomp.ac.cn (A. Kotb), guo@optics.rochester.edu (C. Guo).

https://doi.org/10.1016/j.optlastec.2018.11.048
Received 21 July 2018; Received in revised form 26 October 2018; Accepted 24 November 2018

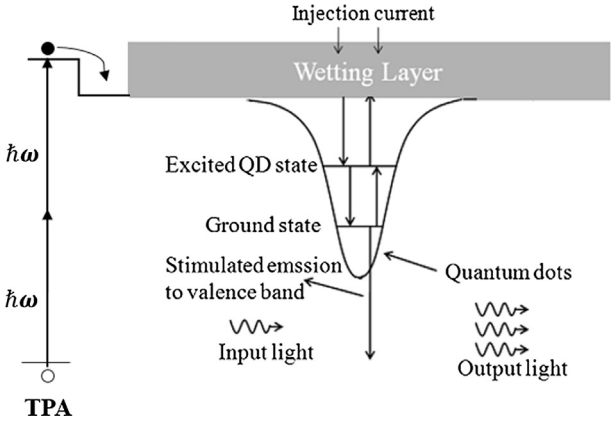

Fig. 1. Diagram of QDs energy levels and carrier transition used for QDSOA modeling with TPA process.

quality factor (QF) on the input signal and QDSOA critical parameters is theoretically examined. For comparison, the results have been obtained for the considered AO gates using QDSOAs with TPA and without TPA at 2 Tb/s The outcome of this study reveals that exploiting TPA in QDSOA allows achieving operation of the considered AO gates at 2 Tb/s both with logical correctness and high quality, essentially doubling the data rate theoretically achieved in previous works [47–50].

The rest of this paper is organized as follows: In Section 2, the QDSOA modeling is formulated. In Section 3, the AND operation principle and the simulation results are described. In Section 4, the OR operation principle and the simulation results are presented. In Section 5, the NAND operation principle and the simulation results are described. Finally, the concluding remarks are given in Section 6.

2. QDSOA modeling

The semiconductor material in the QDSOAs is the commonly employed InAs/GaAs, with InAs QDs embedded in a GaAs layer. The active layer of the device consists of alternately stacked InAs island layers and GaAs intermediate layers [49]. The schematic diagram of the QD physical system with TPA process is shown in Fig. 1. During the amplification process, carriers in QDs that have been depleted by gain bleaching are refilled by carriers generated in the bulk region due to TPA on ultrafast timescales by carrier-relaxation via the WL. The TPA-induced optical pumping provides extra carriers, besides those offered through electrical pumping, to the WL, thus enhancing the rate of carrier capture into the QDs and leading to much reduction and qualitative modification of the carrier recovery dynamics in the QDs [51].

In order to simulate the carrier densities and transitions that affect the QDSOA device gain dynamics, a two-level model is applied [17]. In this computational model, the transitions resulting in photon emission take place from the QDs states conduction band to the valence band. Barrier dynamics [51] are ignored and it is assumed that the WL serves as the only recipient of the injection current [52]. Carriers produced in the WL via the injection current make the transition to the excited state, which acts as the carrier reservoir, followed by a transition to the ground state, which has ultrafast relaxation of carriers whose density determines the device gain.

The effect of 'Carrier Heating' (CH) results from carriers' thermalization in the entire energy band following the pulse. This process is very fast, as it occurs on a time scale between 0.1 ps and 0.7 ps. The pulse energy reduces the optical gain at the photon energy of this excitation and burns a hole in the gain spectrum, which is a process known as 'Spectral Hole Burning' (SHB). By taking into account both CH and SHB effects, the time-dependent gain of a QDSOA is described by the following coupled first-order differential equations [47–50]:

$$\frac{dh_d(t)}{dt} = \frac{h_w(t)}{\tau_{dw}}\left(1 - \frac{h_d(t)}{h_0}\right) - \frac{h_d(t)}{\tau_{dr}} - (exp[h_d(t) + h_{CH}(t) + h_{SHB}(t)] - 1)\frac{P_{in}(t)}{E_{sat}} \quad (1)$$

$$\frac{dh_w(t)}{dt} = \frac{h_{in}}{\tau_{wr}}\left(1 - \frac{h_w(t)}{h_0}\right) - \frac{h_w(t)}{\tau_{wr}} - \frac{h_w(t)}{\tau_{wd}}\left(1 - \frac{h_d(t)}{h_0}\right) \quad (2)$$

$$\frac{dh_{CH}(t)}{dt} = \frac{h_{CH}(t)}{\tau_{CH}} - \frac{\varepsilon_{CH}}{\tau_{CH}}(exp[h_d(t) + h_{CH}(t) + h_{SHB}(t)] - 1)P_{in}(t) \quad (3)$$

$$\frac{dh_{SHB}(t)}{dt} = -\frac{h_{SHB}(t)}{\tau_{SHB}} - \frac{\varepsilon_{SHB}}{\tau_{SHB}}(exp[h_d(t) + h_{SHB}(t) + h_{CH}(t)] - 1)P_{in}(t) - \frac{dh_d(t)}{dt} - \frac{dh_{CH}(t)}{dt} \quad (4)$$

$$h_{in} = \int_0^z \frac{a J \tau_{wr}}{ed} dz' \quad (5)$$

where function 'h' represents QDSOA power gain integrated over the longitudinal dimension, z, for carriers recombination between QDs states (h_d) and WL (h_w), carrier heating (h_{CH}), and spectral hole burning (h_{SHB}). $h_0 = \ln[G_0]$, where G_0 is the unsaturated power gain and E_{sat} is the saturation energy. P(t) is the input power. τ_{dw} is the excitation rate from QD ground state to WL and τ_{dr} is the recombination rate of QD. τ_{wd} is the transition rate from WL to QD ground state and τ_{wr} is the carrier recombination rate of WL. τ_{CH} and τ_{SHB} are the temperature relaxation rate and the carrier-carrier scattering rate, respectively. ε_{CH} and ε_{SHB} are the nonlinear gain suppression factors due to CH and SHB, respectively. α is the differential gain, which represents the ratio of carriers in WL and QDs, J is the injection current density, d is the WL thickness, and e is the electron charge. The total phase of the QDSOA including TPA effect is given by [27–30]:

$$\Phi(t) = -0{\cdot}5(\alpha\, h(t) + \alpha_{CH} h_{CH}(t) + \beta\alpha_{TPA} LS(t)) \quad (6)$$

where α is the traditional linewidth enhancement factor (α-factor), α_{CH} and α_{SHB} are the CH and SHB alpha-factors, respectively, α_{TPA} is the TPA linewidth enhancement factor and β is the TPA coefficient. L is the length of the QDSOA active region, and S(t) is the photon density, which is linked to light power through the relevant conversion factor [24]. Because the TPA phase modulation factor is negative (see Table 1), the phase change due to TPA is in the opposite direction to the phase change due to QDSOA gain.

The input signals are assumed to have a Gaussian-like power profile in the time domain, i.e.

$$P_{A,B,Clk}(t) \equiv P_{in}(t) = \sum_{n=1}^{N} a_{n(A,B),Clk} \frac{2\sqrt{\ln(2)}\, E_0}{\sqrt{\pi}\, \tau_{FWHM}} \exp\left[-\frac{4\ln(2)(t - n\,T)^2}{\tau_{FWHM}^2}\right] \quad (7)$$

where $\alpha_{n(A,B),Clk}$, which can take the logical value '1' or '0' for a_n-long pseudorandom binary sequence (PRBS) of data 'A' and 'B', and '1' for a signal of repetitive pulses, i.e. Clock ('Clk'), of single pulse energy (E_0), bit period (T), and full-width at half-maximum (FWHM) pulse width (τ_{FWHM}). All simulations have been carried out by Mathematica® using the default parameters values cited in Table 1. The performance of the considered AO operations using QDSOA-MZI at 2 Tb/s has been evaluated by the QF, which is defined as $Q = (P_1 - P_0)/(\sigma_1 + \sigma_0)$, where $P_{1,0}$ and $\sigma_{1,0}$ are the average powers and corresponding standard deviations, respectively, of switched pulses binary values '1' & '0'. The dependence of the QF on the input signal and QDSOA critical parameters has been examined and reported in the following sections.

Table 1
Critical parameters calculation values.

Symbol	Definition	Value	Unit	Ref.
E_0	Pulse energy	0.4	pJ	
τ_{FWHM}	Pulse width	0.2	ps	[27]
T	Bit period	0.5	ps	
n	PRBS length	127	–	[48–50]
λ_A	Wavelength of data A	1550	nm	
λ_B	Wavelength of data B	1556	nm	
$\Delta\tau$	Time delay (AND operation)	0.1	ps	
$\Delta\tau_{DI}$	DI delay (OR operation)	0.1	ps	
$\Delta\Phi$	DI phase bias	π	rad	[17]
β	TPA coefficient	20	cm/GW	[53]
α_{TPA}	TPA linewidth enhancement factor	−4	–	[54–56]
J	Injection current density	50	kA/cm^2	
P_{sat}	Saturation power	30	mW	
τ_{wd}	Transition rate from WL to QDs state		ps	[48–50]
τ_{dw}	Excitation rate from QDs state to WL	10	ns	[48–50]
τ_{wr}	Carrier recombination rate in WL	2.2	ns	[48–50]
τ_{dr}	Carrier recombination rate in QDs state	0.4	ns	[48–50]
τ_{CH}	Temperature relaxation rate	0.3	ps	[48–50]
τ_{SHB}	Carrier-carrier scattering rate	0.1	ps	[48–50]
α	Traditional α-factor		–	[32]
α_{CH}	CH α-factor	1	–	[17]
α_{SHB}	SHB α-factor	0	–	[32]
ε_{CH}	CH nonlinear gain suppression factor	0.02	W^{-1}	[48–50]
ε_{SHB}	SHB nonlinear gain suppression factor	0.02	W^{-1}	[48–50]
Γ	Confinement factor	0.15	–	[33,57]
a	Differential gain	8.6×10^{-15}	cm^{-2}	[58]
L	Length of QDSOA active region	1.0	mm	[34]
w	Thickness of QDSOA active region	0.3	μm	[41]
G_0	Unsaturated power gain	20	dB	[32]
N_{SP}	Spontaneous emission factor	2	–	

3. AND gate

3.1. Operation principle

The schematic design and truth table of the all-optical AND gate using QDSOA-MZI is shown in Fig. 2.

Data A and its delayed replica are injected into QDSOA1 and QDSOA2 at MZI upper and lower arms, respectively. Data B, which is spectrally located at a different wavelength so that it can be discriminated from data A versions and combined with the latter using wavelength selective couplers (WSCs), is injected into the middle MZI arm and is equally divided by a 3 dB optical coupler (OC). Data A and its delayed copy open a phase gate for data B [1]. When A = '0' and B = '1' or '0', this phase gate does not exist and the output should be '0'. When both A and B are '1', the phase gate makes the split counterparts of signal B interfere constructively at the output, which therefore results in a switched value of 1. Thus a logical '1' is obtained at the MZI output

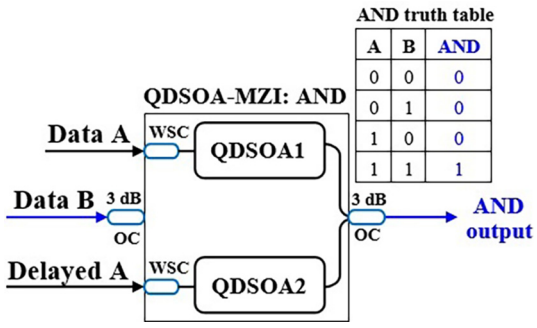

Fig. 2. Schematic design and truth table of AND gate using QDSOA-MZI. OC: 3 dB Optical Coupler. WSC: Wavelength Selective Coupler.

only when both data A and B are '1', which is functionally the same as an all-optical AND gate.

3.2. Simulation

For the AND operation, the total power going into QDSOA1 and QDSOA2 is given by:

$$P_{in,QDSOA1}(t) = P_A(t) + 0.5P_B(t) \tag{8}$$

$$P_{in,QDSOA2}(t) = 0{\cdot}5P_B(t) + P_A(t - \Delta\tau) \tag{9}$$

where $P_A(t)$ and $P_B(t)$ are the powers of data streams A and B, respectively, and $\Delta\tau$ is the temporal offset of delayed signal A.

The QDSOA-MZI output power is described by the following interferometric equation [17]:

$$P_{AND}(t) = 0.25P_B(t)(G_{QDSOA1}(t) + G_{QDSOA2}(t) - 2\sqrt{G_{QDSOA1}(t)\,G_{QDSOA2}(t)}\cos[\Phi_{QDSOA1}(t) - \Phi_{QDSOA2}(t)]) \tag{10}$$

where $G_{QDSOA1,2}(t)$ and $\Phi_{QDSOA1,2}(t)$ are the time-dependent gains and phase changes induced in the two arms of the QDSOA-MZI.

Figs. 3 and 4 show the simulation results for the logic pulse profiles and eye diagrams for the all-optical AND operation using QDSOA-MZI without TPA and with TPA at 2 Tb/s. The peak amplitude fluctuations, which are otherwise observed in the switched pulses, are suppressed in the presence of TPA owing to the enhancement of the carrier recovery dynamics in the QDs [51]. This difference is reflected on the corresponding eye diagram, which subjects to TPA acquires a single border instead of deformed sub-envelopes. These results show that owing to TPA it is possible to realize the specific Boolean operation with pattern-free logical correctness and with a higher QF than without TPA. These results show that owing to TPA it is possible to realize the specific Boolean operation with pattern-free logical correctness and with a higher QF than without TPA, i.e. 17 vs. 9.

The dependence of the QF on the pulse energy and the injection current density has been calculated with TPA and without TPA for AND operation using QDSOA-MZI at 2 Tb/s as shown, respectively, in Fig. 5(a) and (b). We can see from Fig. 5(a) that in the presence of TPA the QF is always higher than without TPA. Physically this happens because in the absence of TPA a high energetic pulse depletes via stimulated emission the QDSOA carrier density, which needs longer time to recover to its initial, unsaturated level. This, in turn, causes a stronger pattern effect and accordingly QF degradation. In the presence of TPA, on the other hand, the carrier density depleted by high energetic pulses recovers faster owing to the TPA-induced extra carriers offered via the WL to those generated by the injection current [51]. This situation occurs up to a certain pulse energy level (≈ 0.8 pJ), beyond which the QF starts to drop due to the shift of the amount of incurred differential phase beyond the vicinity of π (or odd integers of it), where it should lie for proper switching [59]. Similarly, and as shown in Fig. 5(b), the QF is increased with the injection current (for a given active region area) since more carriers are injected into the QDs, thereby allowing for faster refilling and recovery after being depleted by a sufficiently strong pulse that undergoes amplification and switching. This fact considerably reduces the pattern effect and results in higher QF.

Fig. 6 shows the QF of the AND operation as a function of the pulse width and the transition rate from WL to QD ground state (τ_{wd}), with TPA and without TPA, using QDSOA-MZI at 2 Tb/s. The QF is decreased for broader pulses of fixed energy. In this case pulses become less intense in peak amplitude, which makes TPA manifest less strongly. Still, the QF is more tolerant to the increase of pulses temporal content since it remains acceptable across almost the whole scanned range of the examined operating parameter. A similar trend is observed for the QF against τ_{wd}, as shown in Fig. 6(b). The dynamic gain perturbation

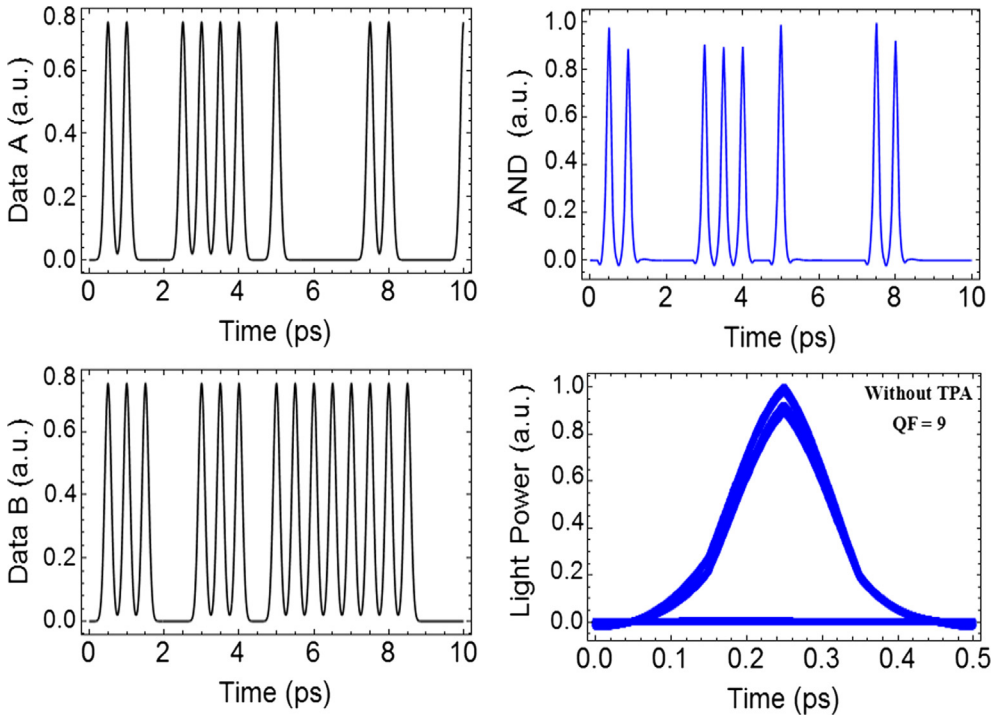

Fig. 3. Simulation results for AND operation without TPA in QDSOAs at 2 Tb/s.

process is accelerated when τ_{wd} is shortened, so the QF is improved for smaller values of this parameter, much more when the nonlinear response speed is enhanced by the presence of TPA.

Fig. 7 shows the QF versus the length and thickness of the QDSOA active region for the AND operation with TPA and without TPA at 2 Tb/s. Generally, the QF is higher for longer and thicker active region. The optical gain region is determined by the active region dimensions, which when larger the carrier density is increased, thereby enhancing the QF. These figures clearly show that the performance of the considered Boolean function is more acceptable with TPA than without TPA.

Fig. 8 shows the dependence of the QF on the confinement factor (Γ) and saturation power (P_{sat}) for the AND operation with TPA and without TPA at 2 Tb/s. For low Γ values, the QF is reduced and also the QF as shown in Fig. 8(a). The similar trend is observed in Fig. 8(b), where the QF against P_{sat}. This figure confirms that the QF inclines with increasing the saturation power. The TPA reduces the pattern effects and results in a higher QF.

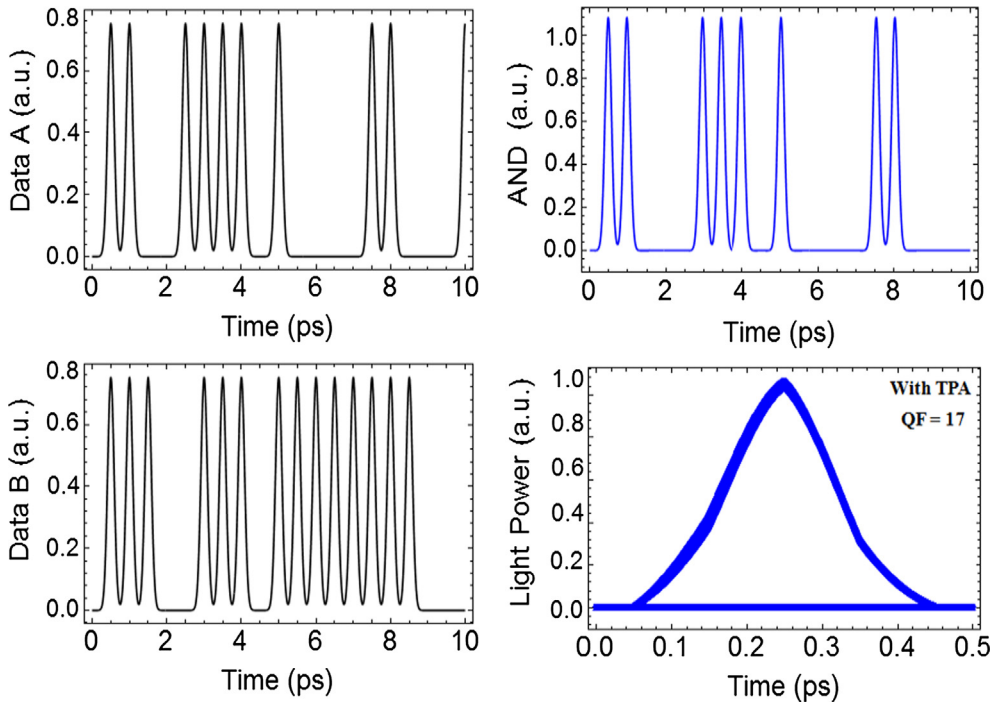

Fig. 4. Simulation results for AND operation with TPA in QDSOAs at 2 Tb/s.

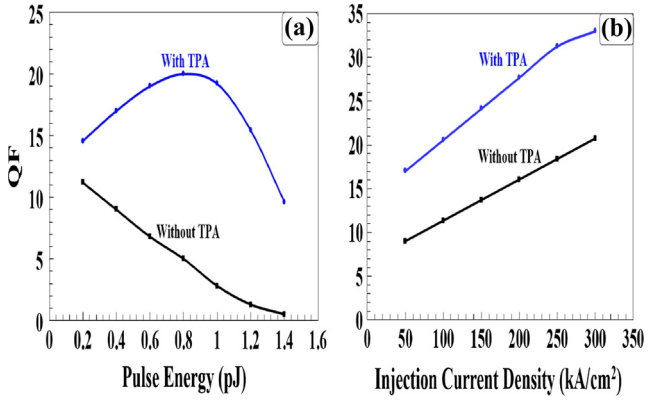

Fig. 5. QF vs. (a) pulse energy and (b) injection current density for QDSOA-based AND operation at 2 Tb/s, with TPA and without TPA.

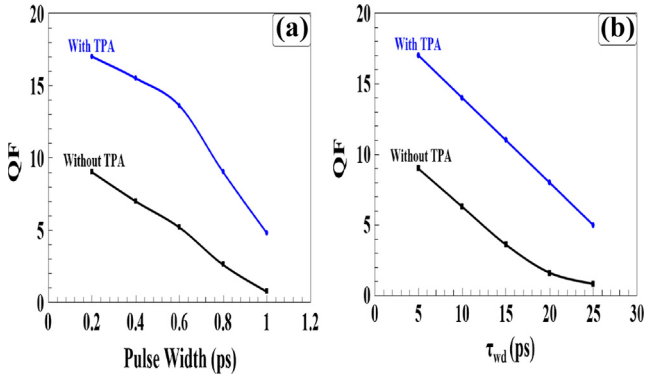

Fig. 6. QF vs. (a) pulse width and (b) transition rate from WL to QDs ground state (τ_{wd}) for QDSOA-based AND operation at 2 Tb/s with TPA and without TPA.

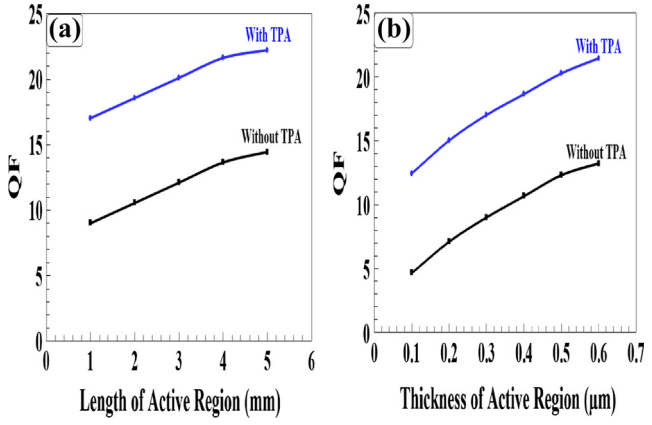

Fig. 7. QF vs. (a) length and (b) thickness of QDSOA active region for AND operation at 2 Tb/s with TPA and without TPA.

4. OR gate

4.1. Operation principle

The schematic design and truth table of the OR gate using QDSOA-DI is shown in Fig. 9 [1,7].

In order to carry-out the OR operation, data streams A, B, and a continuous wave (CW) 'probe' signal are injected into the QDSOA-DI combination. Data A and B induce a phase change on the CW signal via cross-phase modulation in the QDSOA. The CW signal comes out of the QDSOA and is injected into the DI, which has a delay ($\Delta\tau_{DI}$) in one of its arms and a phase bias ($\Delta\Phi$) in the other arm. The DI creates a phase difference between the direct and the temporally offset versions of the CW signal that emerges from the QDSOA and on which the dynamic perturbations by A and B have been mapped. This action opens a phase window whose duration is solely determined by the DI parameter, which is much smaller, i.e. by 5 times, than the target repetition period. This allows the processed pulses preserve the quality of their original profile despite the QDSOA being heavily saturated in the tight driving scenario when both data signals, which must be sufficiently strong so as to efficiently excite the exploited TPA nonlinearity, are present inside the QDSOA. Thus, when A and B are '0', there is no phase change on the CW signal, which results in '0' at the DI output. However, when A or B or both are '1', phase changes are induced on the CW signal and its straightforward and lagging counterparts interfere destructively, which results in '1' at the DI output.

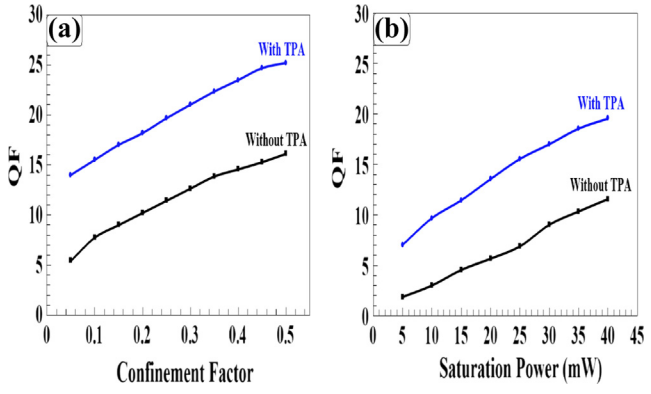

Fig. 8. QF vs. (a) confinement factor and (b) saturation power of QDSOA for AND operation at 2 Tb/s with TPA and without TPA.

4.2. Simulation

The QDSOAs time-dependent gain and phase for the QDSOA-based OR operation are described using Eqs. (1), (2), after being modified by neglecting CH and SHB, and (5). In this case, the total input power, $P_{in}(t)$, inside QDSOA-DI is given by:

$$P_{in,QDSOA-DI}(t) = P_A(t) + P_B(t) + P_{CW} \tag{11}$$

The output power from the DI is given by:

$$P_{OR}(t) = 0.25\,(P_{out}(t) + P_{out}(t-\Delta\tau_{DI}) - 2\sqrt{P_{out}(t)P_{out}(t-\Delta\tau_{DI})}\,\cos[\Phi(t) - \Phi(t-\Delta\tau_{DI}) + \Delta\Phi]) \tag{12}$$

where $P_{out}(t)$ is the output power from the QDSOA, while the cosine argument denotes the differential phase introduced by the DI.

The simulation results for the logic pulse profiles and eye diagrams for the OR operation using QDSOA-DI without and with TPA at 2 Tb/s are shown in Figs. 10 and 11, respectively. Because the single QDSOA employed in the OR gate design is driven into deep saturation by the simultaneous launching of three different signals, it is hard for its perturbed gain to timely recover as much as possible and to a uniform level. This natural difficulty impedes the logic '0's from being fully suppressed and be efficiently distinguished from the logic '1's. As a consequence, without TPA pulses appear at bits slots where both data are empty, when they should not, which distorts the eye diagram. In contrast, with TPA the process of gain recovery is enhanced to the point that these ghost pulses are completely extinguished, thus making the corresponding binary trace lie at perfect zero ground. In this way, the obtained QF is almost twice that without TPA, i.e. 15 vs. 8.2.

The QF as a function of the pulse energy and the injection current density has been calculated with TPA and without TPA for OR operation using QDSOA-MZIs at 2 Tb/s as shown, respectively, in Fig. 12(a)

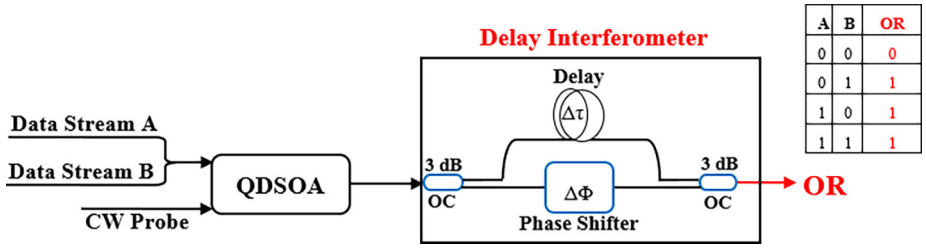

Fig. 9. Schematic design and truth table of OR gate using QDSOA-DI. OC 3 dB Optical Coupler.

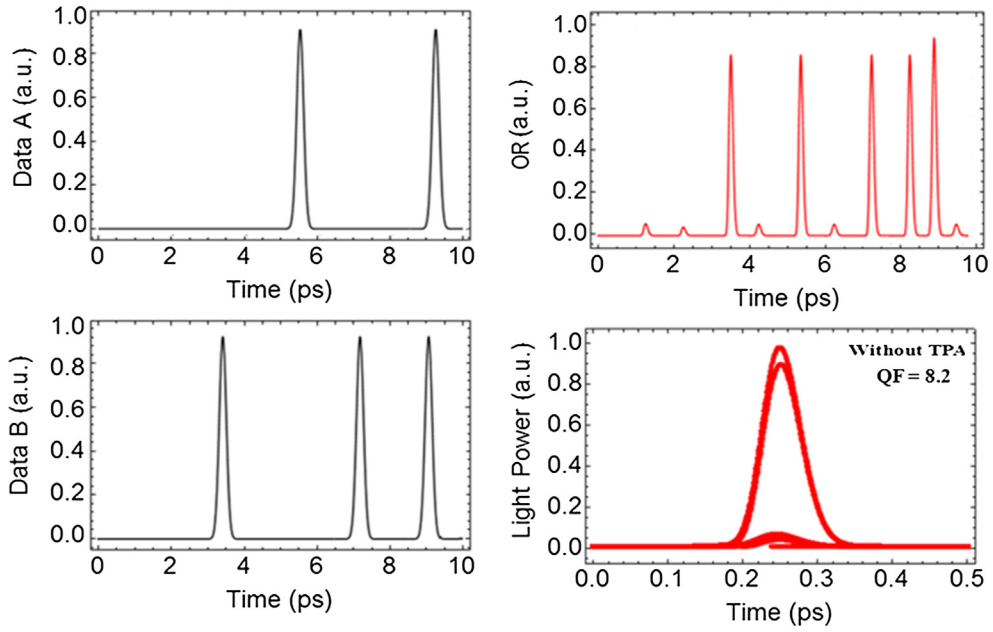

Fig. 10. Simulation results for OR operation without TPA in QDSOA at 2 Tb/s.

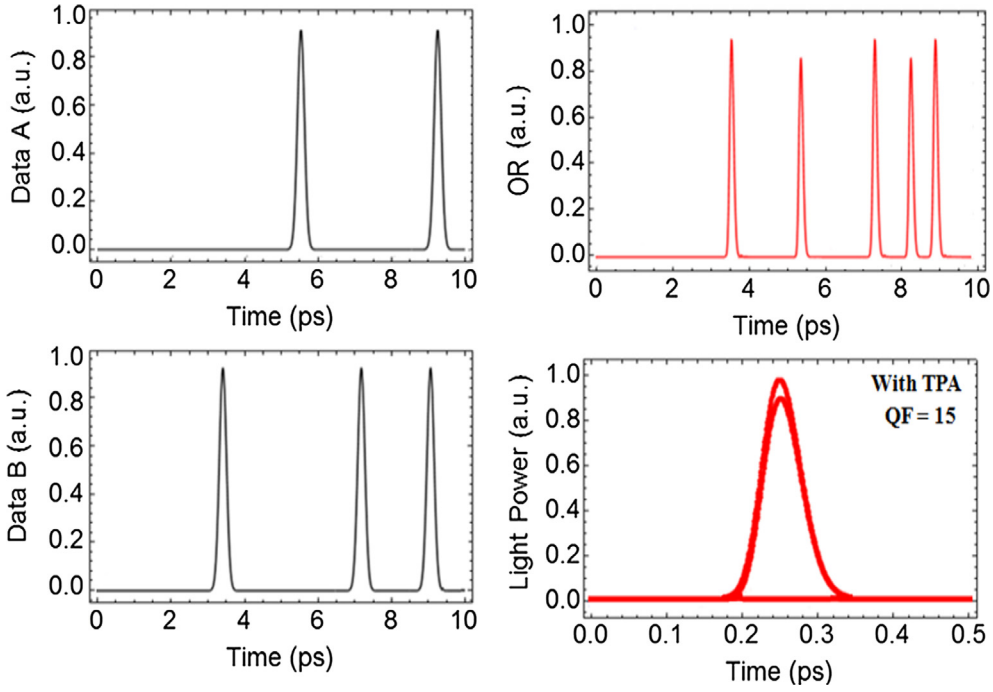

Fig. 11. Simulation results for OR operation with TPA in QDSOA at 2 Tb/s.

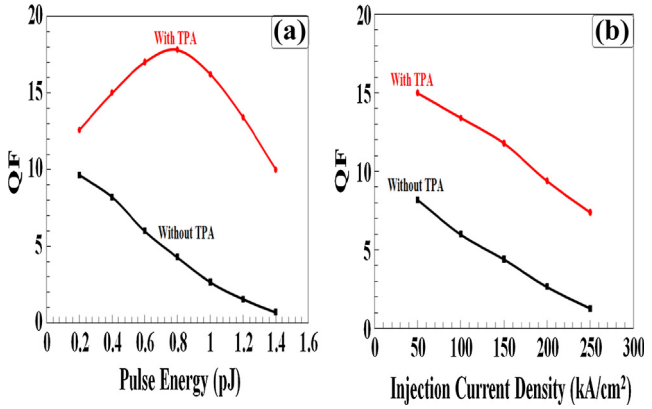

Fig. 12. QF vs. (a) pulse energy and (b) injection current density for QDSOA-based OR operation at 2 Tb/s with TPA and without TPA.

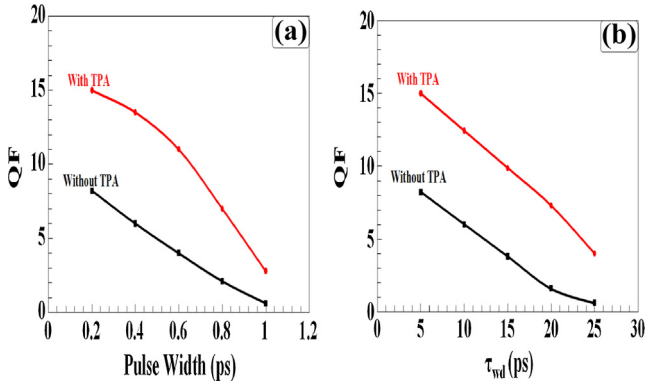

Fig. 13. QF vs. (a) pulse width and (b) transition rate from WL to QDs ground state (τ_{wd}) for QDSOA-based OR operation at 2 Tb/s with TPA and without TPA.

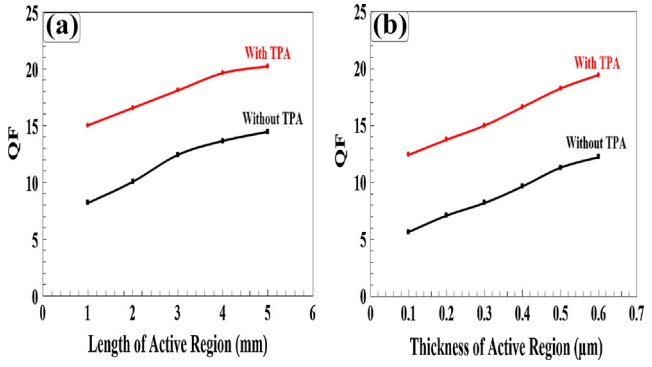

Fig. 14. QF vs. (a) length and (b) thickness of QDSOA active region for OR operation at 2 Tb/s with TPA and without TPA.

and (b).

The dependence of the QF on the pulse width and the transition rate from WL to QDs ground state (τ_{wd}) with TPA and without TPA for QDSOA-DI-based OR operation at 2 Tb/s is shown in Fig. 13(a) and (b), respectively.

The QF as a function of the length and thickness of the QDSOA active region for the OR operation at 2 Tb/s with TPA and without TPA is shown in Fig. 14(a) and (b), respectively.

Fig. 15 shows the QF dependence on the QDSOA confinement factor and saturation power for the OR operation at 2 Tb/s with TPA and without TPA.

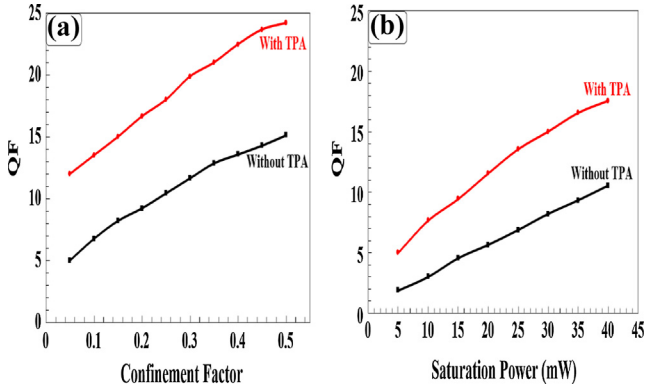

Fig. 15. QF vs. (a) confinement factor and (b) saturation power of QDSOA for OR operation at 2 Tb/s with TPA and without TPA.

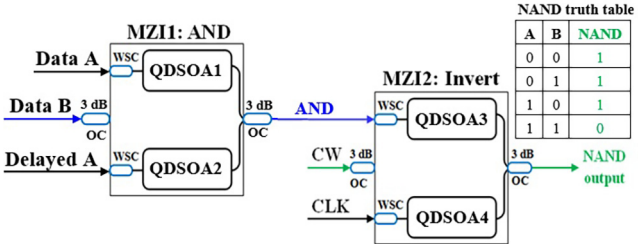

Fig. 16. Schematic design and truth table of NAND gate using QDSOA-MZI. OC: 3 dB Optical Coupler. WSC: Wavelength Selective Coupler.

5. NAND gate

5.1. Operation principle

The schematic design and truth table of the NAND gate using QDSOA-MZI are shown in Fig. 16.

The NAND operation has been carried-out by serially combining AND and INVERT gates, which, as shown in Fig. 16, are realized by 2 MZIs, i.e. MZI1 and MZI2, respectively. The AND output, which has already been realized in Section 3, is guided into MZI2 for undergoing the Invert operation. A clock pulse (CLK) is simultaneously injected into the lower MZI2 arm, while a CW light is injected into the middle MZI2 arm. In this way, the outcome of A NAND B logic is obtained from MZI2 output [49].

5.2. Simulation

The input powers in MZI2 that execute the 'Invert' logic operation are described by:

$$P_{in,\,QDSOA3}(t) = P_{AND}(t) + 0.5P_{CW} \tag{13}$$

$$P_{in,\,QDSOA4}(t) = 0.5P_{CW} + P_C(t) \tag{14}$$

while the NAND output power is given by the following expression:

$$P_{NAND}(t) = 0.25\,P_{CW}\,(G_{QDSOA3}(t) + G_{QDSOA4}(t) - 2\sqrt{G_{QDSOA3}(t)\,G_{QDSOA4}(t)}\,\cos\,[\Phi_{QDSOA3}(t) - \Phi_{QDSOA4}(t)]) \tag{15}$$

The simulation results for the logic pulse profiles and eye diagrams for the NAND operation using QDSOA-MZIs without and with TPA at 2 Tb/s are shown in Figs. 17 and 18, respectively. The achieved QF is 7 without TPA and 13 with TPA. Furthermore, although the pulse an eye shapes are distorted without TPA, nevertheless with TPA they are restored to resemble that of the input data.

The QF of the NAND operation as a function of the pulse energy and

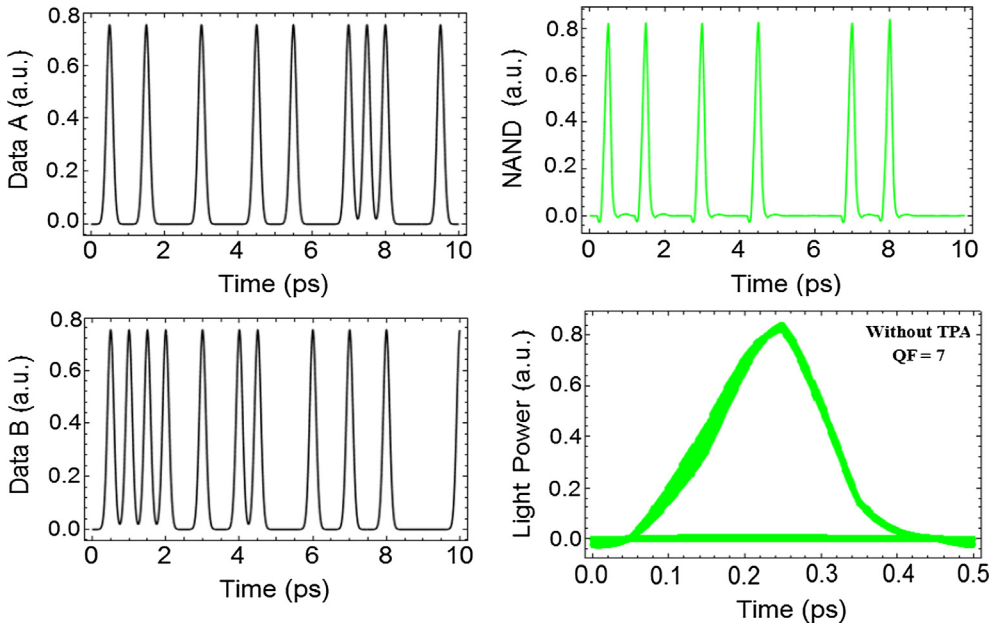

Fig. 17. Simulation results for NAND operation without TPA in QDSOAs at 2 Tb/s.

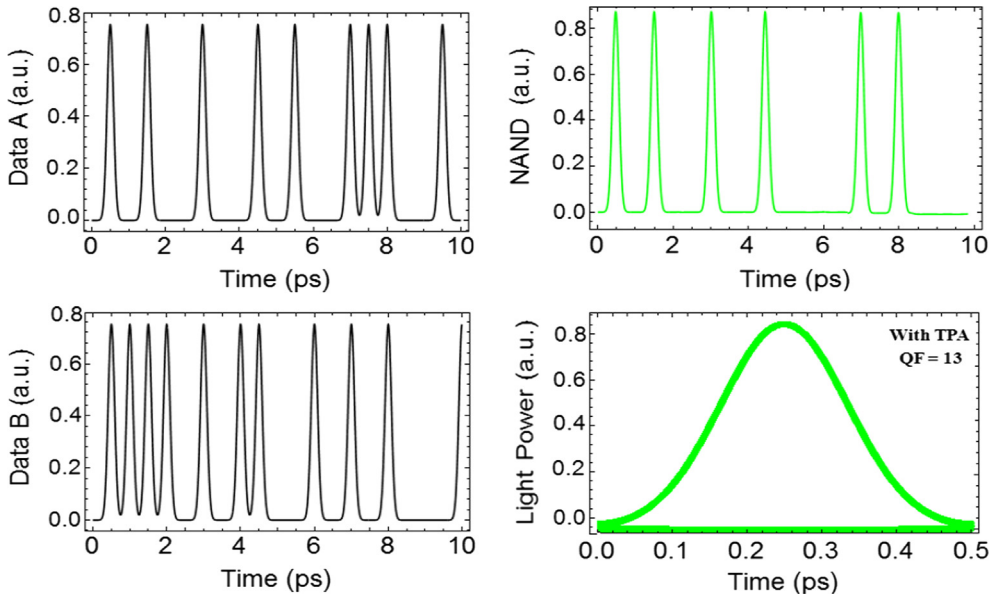

Fig. 18. Simulation results for NAND operation with TPA in QDSOAs at 2 Tb/s.

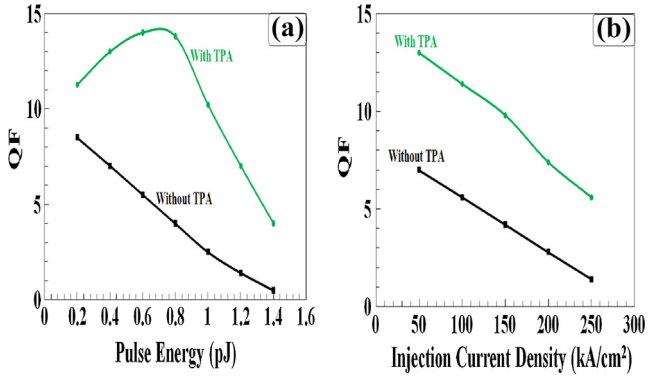

Fig. 19. QF vs. (a) pulse energy and (b) injection current density for QDSOA-based NAND operation at 2 Tb/s with TPA and without TPA.

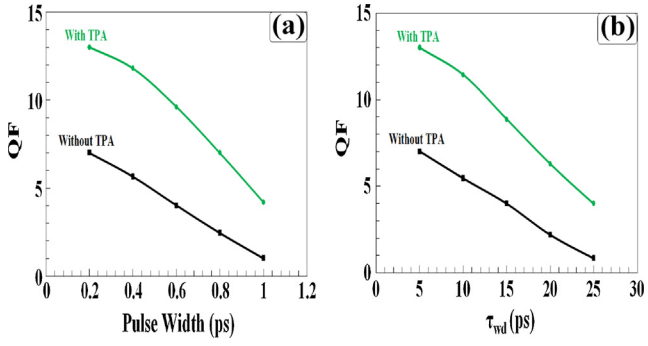

Fig. 20. QF vs. (a) pulse width and (b) transition rate from WL to QDs ground state (τ_{wd}) for QDSOA-based NAND operation at 2 Tb/s with TPA and without TPA.

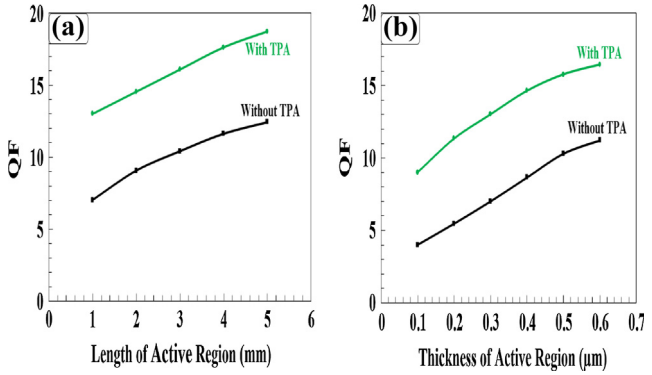

Fig. 21. QF vs. (a) length (b) thickness of QDSOA active region for NAND operation at 2 Tb/s with TPA and without TPA.

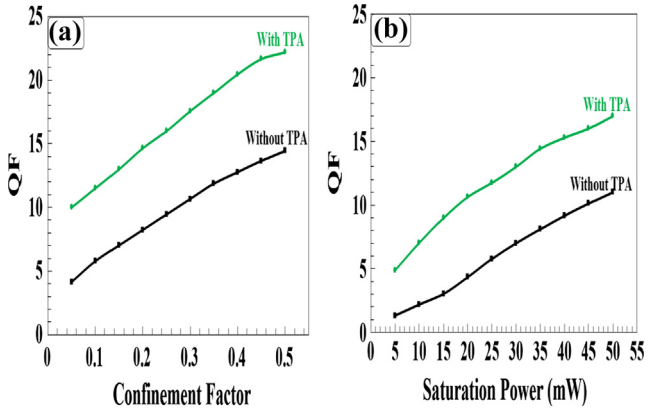

Fig. 22. QF vs. (a) confinement factor (b) saturation power of QDSOA active region for NAND operation at 2 Tb/s with TPA and without TPA.

Table 2
Comparison of different (QD)SOA-based schemes and data rates of theoretically implemented all-optical AND, OR, and NAND gates.

Operation	Scheme	Data rate (Gb/s)	QF	Ref.
AND	SOA	80	7	[4]
	SOA-TPA	250	10.8	[27]
	QDSOA	1000	40.2	[50]
	QDSOA	2000	9	This work
	QDSOA-TPA	2000	17	This work
OR	SOA	80	5.48	[1]
	SOA-TPA	250	9	[31]
	QDSOA	1000	45.5	[50]
	QDSOA	2000	8.2	This work
	QDSOA-TPA	2000	15	This work
NAND	SOA	80	7	[13]
	SOA-TPA	250	8.2	[27]
	QDSOA	1000	36	[49]
	QDSOA	2000	7	This work
	QDSOA-TPA	2000	13	This work

the injection current density with TPA and without TPA is shown, respectively, in Fig. 19(a) and (b) using QDSOA-MZIs at 2 Tb/s. These results have been obtained in the same way as described for AND and OR operations.

The dependence of the QF on the pulse width and the transition rate from WL to QD ground state (τ_{wd}) with TPA and without TPA for QDSOA-MZIs-based NAND operation at 2 Tb/s is shown in Fig. 20 (a) and (b), respectively.

Fig. 21 shows the QF dependence on the length and thickness of the QDSOA active region for the NAND operation at 2 Tb/s with TPA and without TPA.

Fig. 22 shows the QF dependence on the QDSOA confinement factor and saturation power for NAND operation at 2 Tb/s with TPA and without TPA.

Table 2 lists different schemes and data rates of theoretically implemented all-optical AND, OR, and NAND gates reported in the literature. Specifically, the AND and NAND operations have been realized with (QD)SOA-based MZIs, while the OR operation by means of QDSOA and DI combination. It is clearly observed that the higher QF values are obtained when TPA is taken into account as a nonlinear effect in SOAs and QDSOAs modeling, where the latter case further exhibits the best performance in terms of the employed metric, as it has actually been demonstrated in this work. According to the same table, the presence of TPA is also beneficial for speeding up the data rate of these Boolean functions.

The cost of the employed scheme is mainly attributed to the very high input data peak power required to stimulate TPA and exploit it to achieve switching. According to Figs. 5, 12 and 20(a) (as in the old version of this manuscript), the order of this power amounts to ~30 dBm, which can be practically supplied by Erbium Ytterbium-Doped Fiber Amplifiers (EYDFA) designed to exhibit such high output power [60], at the expense of a) significantly higher price of off-the-shelf modules, which can be as high as ~5 times, compared to conventional EDFAs (see for instance https://www.oequest.com/cat/1983, and b) significantly higher power consumption, which can be as high as ~15 times, to account for the electrical and cooling power of the laser diodes used as pump sources [61]. Overall, leveraging TPA to realize the considered all-optical logic gates is accompanied by inevitable financial as well as technical cost, which nevertheless is affordable and justified by the doubling in their operating data rate with more than acceptable performance.

The experimental demonstration of the proposed logic structures would require to control a) the level of the input data peak power, and b) the degree of phase difference between the MZI arms, so that in both cases conditions favorable for switching can be created. This is not a fundamental obstacle but rather a technical matter, which however can be tackled in practice. As mentioned above, issue a) can be addressed using EYDFA, which are commercially available. For b), on the other hand, the differential phase should be fine adjusted to lie in the proper interval according to the binary combination of the input data and the logic outcome expected from the truth table of each target gate [62]. This can be done by employing after each QD-SOA active phase shifters to provide an extra phase difference between the upper and lower MZI arms [63] for achieving optimum switching. From a technological perspective, these shifters are thermo-optic elements which feature low tuning voltage and power dissipation [64] and can be embedded with SOA-based devices in the same planar lightwave circuit platform [65].

6. Conclusion

The performance of Boolean AND, OR, and NAND functions taking into account two-photon absorption (TPA) nonlinear effect in quantum dot semiconductor optical amplifiers (QDSOAs), which are either incorporated in properly configured Mach-Zehnder Interferometers or combined with a Delayed Interferometer, has numerically been investigated at 2 Tb/s. The obtained simulation results suggest that these Boolean functions can be realized at 2 Tb/s better with, than without, TPA being exploited in QDSOAs.

References

[1] H. Dong, Q. Wang, G. Zhu, J. Jaques, A.B. Piccirilli, N.K. Dutta, Demonstration of all-optical logic OR gate using semiconductor optical amplifier-delayed interferometer, Opt. Commun. 242 (2004) 479–485.
[2] N.K. Dutta, Q. Wang, H. Dong, H. Sun, J. Jaques, Semiconductor optical amplifier based photonic logic devices, Proc. SPIE 5814 (2005) 1–8.
[3] N.K. Dutta, J. Jaques, Semiconductor optical amplifier based optical logic devices, Proc. SPIE 6014 (2005) 1–9.

[4] H. Dong, H. Sun, Q. Wang, N.K. Dutta, J. Jaques, 80 Gb/s All-optical logic AND operation using Mach-Zehnder interferometer with differential scheme, Opt. Commun. 265 (2006) 79–83.
[5] A. Sharaiha, J. Topomondzo, P. Morel, All-optical logic AND-NOR gates with three inputs based on cross-gain modulation in a semiconductor optical amplifier, Opt. Commun. 265 (2006) 322–325.
[6] H. Dong, H. Sun, Q. Wang, N.K. Dutta, J. Jaques, All-optical logic AND operation at 80 Gb/s using semiconductor optical amplifier based Mach-Zehnder interferometer, Microwave Opt. Technol. Letts. 48 (2006) 1672–1675.
[7] Q. Wang, H. Dong, H. Sun, N.K. Dutta, All-optical logic OR gate using SOA delayed interferometer, Opt. Commun. 260 (2006) 81–86.
[8] J.Y. Kim, J.M. Kang, T.Y. Kim, S.K. Han, All-optical multiple logic gates with XOR, NOR, OR and NAND function using parallel SOA-MZI structures: theory and experiment, Lightwave Technol. 24 (2006) 3392–3399.
[9] J.Y. Kim, J.M. Kang, T.Y. Kim, S.K. Han, 10 Gbits all-optical composite logic gates with XOR, NOR, OR and NAND functions using SOA-MZI structures, Electron. Letts. 42 (2006) 303–307.
[10] J. Dong, X. Zhang, Y. Wang, J. Xu, D. Huang, 40 Gbit/s reconfigurable photonic logic gates based on various nonlinearities in single SOA, Electron. Letts. 43 (2007) 884–886.
[11] J. Dong, X. Zhang, J. Xu, D. Huang, 40 Gb/s all-optical logic NOR and OR gates using a semiconductor optical amplifier: experimental demonstration and theoretical analysis, Opt. Commun. 281 (2008) 1710–1715.
[12] J.M. Martínez, F. Ramos, J. Martí, 10 Gb/s reconfigurable optical logic gate using a single hybrid-integrated SOA-MZI, Fiber Integr. Opt. 27 (2008) 15–20.
[13] A. Kotb, S. Ma, Z. Chen, N.K. Dutta, G. Said, Effect of amplified spontaneous emission on semiconductor optical amplifier based all-optical logic, Opt. Commun. 284 (2011) 5798–5803.
[14] S.K. Garai, P. Ghosh, S. Mukhopadhyay, Analytical approach of developing wavelength encoded AND, NAND and X-OR logic operations and implementation of the theory using semiconductor optical amplifiers, Optik 122 (2011) 569–576.
[15] A. Kotb, All-Optical Logic Gates Using Semiconductor Optical Amplifier, Lambert Academic Publishing, Germany, 2012.
[16] S. Singh, Lovkesh, Ultrahigh-speed optical signal processing logic based on an SOA-MZI, IEEE J. Sel. Top. Quantum Electron. 18 (2012) 970–975.
[17] N.K. Dutta, Q. Wang, Semiconductor Optical Amplifiers, second ed., World Scientific Publishing Company, Singapore, 2013.
[18] G. Wang, X. Yang, W. Hu, All-optical logic gates for 40 Gb/s NRZ signals using complementary data in SOA-MZIs, Opt. Commun. 290 (2013) 28–32.
[19] S. Singh, R. Kaur, R.S. Kaler, Photonic processing for all-optical logic gates based on semiconductor optical amplifiers, Opt. Eng. 53 (2014) 116102.
[20] P. Singh, D.K. Tripathi, S. Jaiswal, H.K. Dixit, Design and analysis of all-optical AND, XOR and OR gates based on SOA-MZI configuration, Opt. Laser Technol. 66 (2015) 35–44.
[21] A. Lovkesh, Marwaha, Implementation of optical logic gates at 160 Gbps using nonlinear effect of single SOA, Opt. Laser Technol. 70 (2015) 112–118.
[22] A. Kotb, K.E. Zoiros, Soliton all-optical logic AND gate with semiconductor optical amplifier-assisted Mach-Zehnder interferometer, Opt. Eng. 55 (2016) 087109.
[23] A. Kotb, Numerically simulation of soliton OR gate with semiconductor optical amplifier-assisted delayed interferometer, Opt. Quant. Electron. 48 (2016) 462.
[24] A. Kotb, Computational analysis of solitons all-optical logic NAND and XNOR gates using semiconductor optical amplifiers, Opt. Quant. Electron. 49 (2017) 281.
[25] I. Rendón-Salgado, R. Gutiérrez-Castrejón, 160 Gb/s all-optical AND gate using bulk SOA turbo–switched Mach-Zehnder interferometer, Opt. Commun. 399 (2017) 77–86.
[26] X. Yang, D. Lenstra, H.J.S. Dorren, Towards all-optical logic operating at 1 Tbit/s using a semiconductor optical amplifier, Proc. European Conference Optical Communication (ECOC), (2002).
[27] A. Kotb, S. Ma, Z. Chen, N.K. Dutta, G. Said, All-optical logic NAND based on two-photon absorption in semiconductor optical amplifiers, Opt. Commun. 283 (2010) 4707–4712.
[28] A. Kotb, S. Ma, Z. Chen, N.K. Dutta, G. Said, All-optical logic NAND based on two-photon absorption, Proc. SPIE Photonic Devices Appl. 7 (2010) 77810D.
[29] S. Ma, A. Kotb, Z. Chen, N.K. Dutta, All-optical logic gates based on two-photon absorption, Proc. SPIE 7750 (2010) 77501L.
[30] A. Kotb, AND based on two-photon absorption in semiconductor optical amplifier, Optoelectron. Letts. 9 (2013) 181–184.
[31] A. Kotb, Ultrafast all-optical logic OR gate based on two-photon absorption with semiconductor optical amplifier-assisted delayed interferometer, Korean Phys. Soc. 68 (2016) 201–205.
[32] S. Ma, Z. Chen, H. Sun, N.K. Dutta, High-speed all-optical logic gates based on quantum dot-semiconductor optical amplifiers, Opt. Express 18 (2010) 6417–6422.
[33] H. Sun, Q. Wang, H. Dong, N.K. Dutta, All-optical logic performance of quantum dot semiconductor amplifier-based devices, Microwave Opt. Technol. Letts. 48 (2006) 29–35.
[34] S. Ma, Z. Chen, H. Sun, N.K. Dutta, High-speed all-optical PRBS generation based on quantum-dot semiconductor optical amplifiers, Opt. Express 17 (2009) 18469–18477.
[35] A. Kotb, NAND gate with quantum-dot semiconductor optical amplifiers-based Mach-Zehnder interferometer, Optoelectron. Letts. 9 (2013) 89–92.
[36] A. Kotb, NOR gate based on QD-SOA at 250 Gbit/s, Opt. Quant. Electron. 45 (2013) 473–480.
[37] A. Kotb, K.E. Zoiros, Simulation of all-optical logic XNOR gate based on quantum-dot semiconductor optical amplifiers with amplified spontaneous emission, Opt. Quant. Electron. 45 (2013) 1213–1222.
[38] A. Kotb, K.E. Zoiros, On the design of all-optical gates based on quantum-dot semiconductor optical amplifier with effect of amplified spontaneous emission, Opt. Quant. Electron. 46 (2014) 977–989.
[39] E. Dimitriadou, K.E. Zoiros, All-optical XOR gate using single quantum-dot SOA and optical filter, Lightwave Technol. 31 (2013) 3813–3821.
[40] E. Dimitriadou, K.E. Zoiros, On the feasibility of 320 Gb/s all-optical AND gate using quantum-dot semiconductor optical amplifier-based Mach-Zehnder interferometer, PIERS B 50 (2013) 113–140.
[41] E. Dimitriadou, K.E. Zoiros, Proposal for ultrafast all-optical XNOR gate using single quantum-dot semiconductor optical amplifier-based Mach-Zehnder interferometer, Opt. Laser Technol. 45 (2013) 79–88.
[42] E. Dimitriadou, K.E. Zoiros, On the design of reconfigurable ultrafast all-optical NOR and NAND gates using a single quantum-dot semiconductor optical amplifier-based Mach-Zehnder interferometer, J. Opt. 14 (2012) 105401/1–9.
[43] E. Dimitriadou, K.E. Zoiros, On the feasibility of ultrafast all-optical NAND gate using single quantum-dot semiconductor optical amplifier-based Mach-Zehnder interferometer, Opt. Laser Technol. 44 (2012) 1971–1981.
[44] E. Dimitriadou, K.E. Zoiros, Proposal for all-optical NOR gate using single quantum-dot semiconductor optical amplifier-based Mach-Zehnder interferometer, Opt. Commun. 285 (2012) 1710–1716.
[45] E. Dimitriadou, K.E. Zoiros, On the design of ultrafast all-optical NOT gate using quantum-dot semiconductor optical amplifier-based Mach-Zehnder interferometer, Opt. Laser Technol. 44 (2012) 600–607.
[46] H.C.H. Mulvad, M. Galili, L.K. Oxenløwe, H. Hu, A.T. Clausen, J.B. Lensen, C. Peucheret, P. Jeppesen, Demonstration of 5.1 Tbit/s data capacity on a single-wavelength channel, Opt. Express 18 (2010) 1438–1443.
[47] M. Sahafi, A. Rostami, A. Sahafi, All-optical high-speed Logic gates using SOA, Opt. Commun. 285 (2010) 2289–2292.
[48] A. Kotb, 1 Tb/s high-quality factor NOR gate based on quantum-dot semiconductor optical amplifier, Opt. Quant. Electron. 45 (2013) 1258–1268.
[49] A. Kotb, K.E. Zoiros, 1 Tb/s high-quality factor NAND gate using quantum-dot semiconductor optical amplifiers in Mach-Zehnder interferometer, Comp. Electron. 13 (2014) 555–561.
[50] A. Kotb, Simulation of high-quality-factor all-optical logic gates based on quantum-dot semiconductor optical amplifier at 1 Tb/s, Optik 126 (2016) 320–325.
[51] H. Ju, A.V. Uskov, R. Notzel, Z. Li, J.M. Vazquez, D. Lenstra, G.D. Khoe, H.J.S. Dorren, Effects of two-photon absorption on carrier dynamics in quantum-dot optical amplifiers, Appl. Phys. B 82 (2006) 615–620.
[52] T.W. Berg, S. Bischoff, I. Magnusdottir, J. Mørk, Ultrafast gain recovery and modulation limitations in self-assembled quantum-dot devices, IEEE Photon. Technol. Letts. 13 (2001) 541–543.
[53] H. Folliot, M. Lynch, A.L. Bradley, T. Krug, L.A. Dunbar, J. Hegarty, J.F. Donegan, Two-photon-induced photoconductivity enhancement in semiconductor micro-cavities: a theoretical investigation, Opt. Soc. Am. B 19 (2002) 2396–2402.
[54] H.J.S. Dorren, G.D. Khoe, D. Lenstra, All-optical switching of an ultrashort pulse using a semiconductor optical amplifier in a Sagnac-interferometric arrangement, Opt. Commun. 205 (2002) 247–252.
[55] H.J.S. Dorren, X. Yang, A.K. Mishra, Z. Li, H. Ju, H. de-Waardt, G.D. Khoe, T. Simoyama, H. Ishikawa, H. Kawashima, T. Hasama, All-optical logic based on ultrafast gain and index dynamics in a semiconductor optical amplifier, IEEE J. Sel. Top. Quantum Electron. 10 (2004) 1079–1092.
[56] H.J.S. Dorren, X. Yang, D. Lenstra, H. de Waart, G.D. Khoe, T. Simoyama, H. Ishikawa, H. Kawashima, T. Hasama, Ultrafast refractive index dynamics in a multi-quantum well semiconductor optical amplifier, IEEE Photon. Technol. Letts. 15 (2003) 792–794.
[57] A. Kotb, K.E. Zoiros, C. Guo, All-optical XOR, NOR, and NAND logic functions with parallel semiconductor optical amplifier-based Mach-Zehnder interferometer modules, Opt. Laser Technol. 108 (2018) 426–433.
[58] T. Akiyama, O. Wada, H. Kuwatsuka, T. Simoyama, Y. Nakata, K. Mukai, M. Sugawara, H. Ishikawa, Nonlinear processes responsible for non-degenerate four-wave mixing in quantum dot optical amplifiers, Appl. Phys. Letts. 77 (2000) 1753–1755.
[59] G. Papadopoulos, K.E. Zoiros, On the design of semiconductor optical amplifier-assisted Sagnac interferometer with full data dual output switching capability, Opt. Laser Technol. 43 (2011) 697–710.
[60] R. Ahmad, S. Chatigny, M. Rochette, Broadband amplification of high power 40 Gb/s channels using multimode Er-Yb doped fiber, Opt. Express 18 (2010) 19983–19993.
[61] S. Jain, C. Castro, Y. Jung, J. Hayes, R. Sandoghchi, T. Mizuno, Y. Sasaki, Y. Amma, Y. Miyamoto, M. Bohn, K. Pulverer, Md. Nooruzzaman, T. Morioka, S. Alam, D.J. Richardson, 32-core erbium/ytterbium-doped multicore fiber amplifier for next-generation space-division multiplexed transmission system, Opt. Express 25 (2017) 32887–32896.
[62] J. Leuthold, P.A. Besse, J. Eckner, E. Gamper, M. Dulk, H. Melchior, All-optical space switches with gain and principally ideal extinction ratios, IEEE J. Quantum Electron. 34 (1998) 622–633.
[63] N.C. Harris, Y. Ma, J. Mower, T. Baehr-Jones, D. Englund, M. Hochberg, C. Galland, Efficient, compact and low loss thermo-optic phase shifter in silicon, Opt. Express 22 (2014) 10487–10493.
[64] J.D. LeGrange, M. Dinu, T. Sochor, P. Bollond, A. Kasper, S. Cabot, G.S. Johnson, I. Kang, A. Grant, J. Kay, J. Jaques, Cascaded all-optical operations in a hybrid integrated 80-Gb/s logic circuit, Opt. Express 22 (2014) 13600–13615.